J|A|C|S
ARTICLES
Published on Web 10/11/2007

Cross-Strand Coupling of a β-Hairpin Peptide Stabilized with an Aib-Gly Turn Studied Using Isotope-Edited IR Spectroscopy

Rong Huang,[†] Vladimir Setnička,[†,§] Marcus A. Etienne,[‡] Joohyun Kim,[†] Jan Kubelka,[†,||] Robert P. Hammer,[‡] and Timothy A. Keiderling*[,†]

Contribution from the Department of Chemistry, University of Illinois at Chicago, 845 West Taylor Street (m/c111), Chicago, Illinois 60607-7061, Department of Chemistry, Louisiana State University, 232 Choppin Hall, Baton Rouge, Louisiana 70803-1804

Received June 4, 2007; E-mail: tak@uic.edu

Abstract: Isotope-edited IR spectroscopy was used to study a series of singly and doubly $^{13}C{=}O$-labeled β-hairpin peptides stabilized by an Aib-Gly turn sequence. The double-labeled peptides have amide I′ IR spectra that show different degrees of vibrational coupling between the ^{13}C-labeled amides due to variations in the local geometry of the peptide structure. The single-labeled peptides provide controls to determine frequencies characteristic of the diagonal force field (FF) contributions at each position for the uncoupled $^{13}C{=}O$ modes. Separation of diagonal FF and coupling effects on the spectra are used to explain the cross-strand labeled spectral patterns. DFT calculations based on an idealized model β-hairpin peptide correctly predict the vibrational coupling patterns. Extending these model results by consideration of frayed ends and the hairpin conformational flexibility yields an alternate interpretation of details of the spectra. Temperature-dependent isotopically labeled IR spectra reveal differences in the thermal stabilities of the individual isotopically labeled sites. This is the first example of using an IR-based isotopic labeling technique to differentiate structural transitions at specific sites along the peptide backbone in model β-hairpin peptides.

Introduction

Studies of structural characteristics of peptide models with ordered secondary structures are important for developing understanding of protein folding.[1,2] Peptide models can show fundamental characteristics of protein folding such as hydrophobic collapse,[3] hydrogen bond (H-bond) formation,[4] and side-chain interaction[5] in a simpler molecular framework which allows isolation of the secondary and tertiary interactions.

Early studies in this field focused on model α-helical peptides using designed peptide sequences to study helix formation and stability.[6−8] By contrast, it has been more difficult to design and realize good β-sheet and/or β-hairpin peptide models due to the intrinsic variability of β-sheet structures (parallel vs antiparallel, in or out of register, twisted or flat). The tendency of monomer structures to aggregate, which is a required property for sheet formation, leads to relatively large and indeterminate sizes.

However, during the past decade, many linear peptide designs were shown to successfully adopt β-hairpin conformations, which have facilitated detailed equilibrium and kinetic studies of β-structures.[9−15] A controversy has developed over the relative importance of hydrophobic collapse and turn formation for initiating and stabilizing hairpin formation. It is generally accepted that characteristic H-bonds form later in the process. Currently there are three major folding mechanisms proposed for β-hairpin formation: The hydrophobic collapse model[16] suggests that the initial step is not due to turn formation but to the condensation of apolar residues. The "zipping" model[17] suggests initial formation of a turn followed by H-bond formation along the backbone. Finally a mixture of these models

[†] University of Illinois at Chicago.
[‡] Louisiana State University.
[§] Current address: Department of Analytical Chemistry, Institute of Chemical Technology, Technicka 5, 166 28 Prague 6, Czech Republic.
[||] Current address: Department of Chemistry, University of Wyoming, Laramie, WY, 82071.

(1) Callender, R. H.; Dyer, R. B.; Gilmanshin, R.; Woodruff, W. H. *Annu. Rev. Phys. Chem.* **1998**, *49*, 173−202.
(2) Eaton, W. A.; Muñoz, V.; Hagen, S. J.; Jas, G. S.; Lapidus, L. J.; Henry, E.; Hofrichter, J. *Annu. Rev. Biophys. Biomol. Struct.* **2000**, *29*, 327−359.
(3) Espinosa, J. F.; Gellman, S. H. *Angew. Chem., Int. Ed.* **2000**, *39*, 2330−2333.
(4) Krantz, B. A.; Moran, L. B.; Kentsis, A.; Sosnick, T. R. *Nat. Struct. Biol.* **2000**, *7*, 62−71.
(5) Syud, F. A.; Stanger, H. E.; Gellman, S. H. *J. Am. Chem. Soc.* **2001**, *123*, 8667−8677.
(6) Rohl, C. A.; Baldwin, R. L. *Methods Enzymol.* **1998**, *295*, 1−26.
(7) Scholtz, J. M.; Baldwin, R. L. *Annu. Rev. Biophys. Biomol. Struct.* **1992**, *21*, 95−118.
(8) Williams, S.; Causgrove, T. P.; Gilmanshin, R.; Fang, K. S.; Callender, R. H.; Woodruff, W. H.; Dyer, R. B. *Biochemistry* **1996**, *35*, 691−697.
(9) Gellman, S. H. *Curr. Opin. Chem. Biol.* **1998**, *2*, 717−725.
(10) Ramírez-Alvarado, M.; Kortemme, T.; Blanco, F. J.; Serrano, L. *Bioorg. Med. Chem.* **1999**, *7*, 93−103.
(11) Nesloney, C. L.; Kelly, J. W. *Bioorg. Med. Chem.* **1996**, *4*, 739−766.
(12) Smith, C. K.; Regan, L. *Acc. Chem. Res.* **1997**, *30*, 153−161.
(13) Stotz, C. E.; Topp, E. M. *J. Pharm. Sci.* **2004**, *93*, 2881−2894.
(14) Searle, M. S.; Ciani, B. *Curr. Opin. Struct. Biol.* **2004**, *14*, 458−464.
(15) Hughes, R. M.; Waters, M. L. *Curr. Opin. Struct. Biol.* **2006**, *16*, 514−524.
(16) Dinner, A. R.; Lazaridis, T.; Karplus, M. *Proc. Natl. Acad. Sci. U.S.A.* **1999**, *96*, 9068−9073.
(17) Muñoz, V.; Henry, E. R.; Hofrichter, J.; Eaton, W. A. *Proc. Natl. Acad. Sci. U.S.A.* **1998**, *95*, 5872−5879.

10.1021/ja0736414 CCC: $37.00

has been proposed.[18] These differences arise from the complex energy landscape for the formation of β-hairpins[19] and the effects of various unique peptide sequences on the relative weights of different contributions to the process.[20−22]

The 16-residue β-hairpin derived from the protein G B1 domain was the first β-hairpin model system widely studied using equilibrium IR spectroscopy[23] and folding kinetics by T-jump fluorescence.[24] Another widely studied β-hairpin model template (Trpzip), which is stabilized by hydrophobic interactions of Trp residues, was proposed by Cochran,[25] and has been studied by IR,[19,26] T-jump IR,[27,28] T-jump fluorescence,[29,30] and 2D-IR.[31,32] We will present results of our isotopic labeling study of Trpzip models separately (Huang et al., to be published). We have previously presented spectra and theoretical models for a series of β-hairpin peptides based on ^{D}Pro-Gly and Asn-Gly turn sequences incorporated into hairpin sequences designed by Gellman.[33] All these studies combined with NMR data provided an increasing understanding of the stability and folding mechanisms of β-hairpin peptides.[34,35]

While for many proteins the thermal unfolding often appears to be a two-state process,[36] for peptides, in many cases, this is not an appropriate model.[26,34,37−42] Although some β-hairpin peptides are reported to favor a two-state transition,[24,43,44] results with various methods indicate a deviation from a "true" two-state transition for several β-hairpin model peptides.[19,34,39,41,45] NMR studies using isotopic labeling on different segments of the peptide sequence provide evidence of multistate unfolding.[38] The lack of two-state signature could be attributed to different factors such as the dynamics of the β-hairpin structure and the effect of the specific sequence on the cooperativity between the β-turn formation and the hydrophobic cluster formation. Kinetic experiments (T-jump IR or T-jump fluorescence) also have some controversy regarding interpretation of the relaxation in terms of a single exponential.[24,46] In response, isotopic labeling can provide useful information to test the overall cooperativity and local stability differences.

Optical spectra are sensitive to rapid structural change and provide data reflecting the population of various intermediate states, if they are spectrally distinct. Infrared (IR) and circular dichroism (CD) spectroscopies are primarily used to monitor secondary structure, and fluorescence is used to follow the tertiary structure change. The disadvantage of these methods is that they are low resolution, having no site selectivity, so that only average structural change is normally monitored. Isotope-edited IR spectroscopy can allow study of the thermal unfolding process in a more site-specific manner, thus yielding a better understanding of the peptide folding mechanism.[37,47]

Isotope-edited IR spectroscopy has become a useful means of developing site-specific structural and dynamic information of polypeptides.[47] It has been used to study structural and coupling information in α-helix conformation,[37,48−50] solvation/desolvation,[51−53] N-capping,[54] stability and unfolding dynamics,[55−57] β-sheet formation and aggregation.[58−66] We have begun a series of studies on β-hairpins using isotopic labeling and vibrational spectra[67−69] for which this paper develops an interpretation of cross-strand coupling. The most stable hairpin turns reported incorporate a non-proteinic ^{D}Pro-Gly sequence[33,70,71]

(18) Felts, A. K.; Narano, Y.; Gallicchio, E.; Levy, R. M. *Proteins* **2004**, *56*, 310−321.
(19) Yang, W.-Y.; Pitera, J. W.; Swope, W. C.; Gruebele, M. *J. Mol. Biol.* **2004**, *336*, 241−251.
(20) Deechongkit, S.; Nguyen, H.; Jager, M.; Powers, E. T.; Gruebele, M.; Kelly, J. W. *Curr. Opin. Struct. Biol.* **2006**, *16*, 94−101.
(21) Colombo, G.; DeMori, G. M. S.; Roccatano, D. *Protein Sci.* **2003**, *12*, 538−550.
(22) Griffiths-Jones, S. R.; Sharman, G. J.; Maynard, A. J.; Searle, M. S. *J. Mol. Biol.* **1998**, *284*, 1597−1609.
(23) Arrondo, J. L. R.; Blanco, F. J.; Serrano, L.; Goni, F. M. *FEBS Lett.* **1996**, *384*, 35−37.
(24) Muñoz, V.; Thompson, P. A.; Hofrichter, J. *Nature* **1997**, *390*, 196−199.
(25) Cochran, A. G.; Skelton, N. J.; Starovasnik, M. A. *Proc. Natl. Acad. Sci. U.S.A.* **2001**, *98*, 5578−5583.
(26) Wang, T.; Xu, Y.; Du, D.; Gai, F. *Biopolymers* **2004**, *75*, 163−172.
(27) Du, D.; Tucker, M. J.; Gai, F. *Biochemistry* **2006**, *45*, 2668−2678.
(28) Du, D.; Zhu, Y.; Huang, C.-Y.; Gai, F. *Proc. Natl. Acad. Sci. U.S.A.* **2004**, *101*, 15915−15920.
(29) Snow, C. D.; Qiu, L.; Du, D.; Gai, F.; Hagen, S. J.; Pande, V. S. *Proc. Natl. Acad. Sci. U.S.A.* **2004**, *101*, 4077−4082.
(30) Yang, W.-Y.; Gruebele, M. *J. Am. Chem. Soc.* **2004**, *126*, 7758−7759.
(31) Smith, A. W.; Chung, H. S.; Ganim, Z.; Tokmakoff, A. *J. Phys. Chem. B* **2005**, *109*, 17025−17027.
(32) Wang, J.; Chen, J.; Hochstrasser, R. M. *J. Phys. Chem. B* **2006**, *110*, 7545−7555.
(33) Stanger, H. E.; Gellman, S. H. *J. Am. Chem. Soc.* **1998**, *120*, 4236−4237.
(34) Hilario, J.; Kubelka, J.; Keiderling, T. A. *J. Am. Chem. Soc.* **2003**, *125*, 7562−7574.
(35) Hilario, J.; Kubelka, J.; Syud, F. A.; Gellman, S. H.; Keiderling, T. A. *Biospectroscopy* **2002**, *67*, 233−236.
(36) Jackson, S. E. *Folding Des.* **1998**, *3*, R81−91.
(37) Silva, R. A. G. D.; Kubelka, J.; Decatur, S. M.; Bour, P.; Keiderling, T. A. *Proc. Natl. Acad. Sci. U.S.A.* **2000**, *97*, 8318−8323.
(38) Santiveri, C. M.; Santoro, J.; Rico, M.; Jimenez, M. A. *J. Am. Chem. Soc.* **2002**, *124*, 14903−14909.
(39) Kuznetsov, S. V.; Hilario, J.; Keiderling, T. A.; Ansari, A. *Biochemistry* **2003**, *42*, 4321−4332.
(40) Lopez, M. M.; Chin, D.-H.; Baldwin, R. L.; Makhatadze, G. I. *Proc. Natl. Acad. Sci. U.S.A.* **2002**, *99*, 1298−1302.
(41) Ahmed, Z.; Beta, I. A.; Mikhonin, A. V.; Asher, S. A. *J. Am. Chem. Soc.* **2005**, *127*, 10943−10950.
(42) Yamazaki, T.; Furuya, H.; Watanabe, T.; Nishiuchi, Y.; Nishio, H.; Abe, A. *Chem. Today* **2006**, *24*, 55−58.
(43) Espinosa, J. F.; Muñoz, V.; Gellman, S. H. *J. Mol. Biol.* **2001**, *306*, 397−402.
(44) Streicher, W. W.; Makhatadze, G. I. *J. Am. Chem. Soc.* **2006**, *128*, 30−31.
(45) Dhanasekaran, M.; Prakash, O.; Gong, Y.-X.; Baures, P. W. *Org. Biomol. Chem.* **2004**, *2*, 2071−2082.
(46) Xu, Y.; Wang, T.; Gai, F. *Chem. Phys.* **2006**, *323*, 21−27.
(47) Decatur, S. M. *Acc. Chem. Res.* **2006**, *39*, 169−175.
(48) Decatur, S. M.; Antonic, J. *J. Am. Chem. Soc.* **1999**, *121*, 11914−11915.
(49) Barber-Armstrong, W.; Donaldson, T.; Wijesooriya, H.; Silva, R. A. G. D.; Decatur, S. M. *J. Am. Chem. Soc.* **2004**, *126*, 2339−2345.
(50) Huang, R.; Kubelka, J.; Barber-Armstrong, W.; Silva, R. A. G. D.; Decatur, S. M.; Keiderling, T. A. *J. Am. Chem. Soc.* **2004**, *126*, 2346−2354.
(51) Starzyk, A.; Barber-Armstrong, W.; Sridharan, M.; Decatur, S. M. *Biochemistry* **2005**, *44*, 369−376.
(52) Fesinmeyer, R. M.; Peterson, E. S.; Dyer, R. B.; Andersen, N. H. *Protein Sci.* **2005**, *14*, 2324−2332.
(53) Walsh, S. T. R.; Cheng, R. P.; Wright, W. W.; Alonso, D. O. V.; Daggett, V.; Vanderkooi, J. M.; DeGrado, W. F. *Protein Sci.* **2003**, *12*, 520−531.
(54) Decatur, S. M. *Biopolymers* **2000**, *54*, 180−185.
(55) Huang, C. Y.; Getahun, Z.; Wang, T.; DeGrado, W. F.; Gai, F. *J. Am. Chem. Soc.* **2001**, *123*, 12111−12112.
(56) Venyaminov, S. Y.; Hedstrom, J. F.; Prendergast, F. G. *Proteins* **2001**, *45*, 81−89.
(57) Ramajo, A. P.; Petty, S. A.; Starzyk, A.; Decatur, S. M.; Volk, M. *J. Am. Chem. Soc.* **2005**, *127*, 13784−13785.
(58) Brauner, J. W.; Dugan, C.; Mendelsohn, R. *J. Am. Chem. Soc.* **2000**, *122*, 677−683.
(59) Silva, R. A. G. D.; Barber-Armstrong, W.; Decatur, S. M. *J. Am. Chem. Soc.* **2003**, *125*, 13674−13675.
(60) Petty, S. A.; Adalsteinsson, T.; Decatur, S. M. *Biochemistry* **2005**, *44*, 4720−4726.
(61) Petty, S. A.; Decatur, S. M. *Proc. Natl. Acad. Sci. U.S.A.* **2005**, *102*, 14272−14277.
(62) Petty, S. A.; Decatur, S. M. *J. Am. Chem. Soc.* **2005**, *127*, 13488−13489.
(63) Paul, C.; Axelsen, P. H. *J. Am. Chem. Soc.* **2005**, *127*, 5754−5755.
(64) Paul, C.; Wang, J.; Wimley, W. C.; Hochstrasser, R. M.; Axelsen, P. H. *J. Am. Chem. Soc.* **2004**, *126*, 5843−5850.
(65) Lansbury, P. T. J.; Costa, P. R.; Griffiths, J. M.; Simon, E. J.; Auger, M.; Halverson, K. J.; Kocisko, D. A.; Hendsch, Z. S.; Ashburn, T. T.; Spencer, R. G. *Nat. Struct. Biol.* **1995**, *2*, 990−998.
(66) Halverson, K.; Sucholeiki, I.; Ashburn, T. T.; Lansbury, P. T. *J. Am. Chem. Soc.* **1991**, *113*, 6701−6703.
(67) Setnička, V.; Huang, R.; Thomas, C. L.; Etienne, M. A.; Kubelka, J.; Hammer, R. P.; Keiderling, T. A. *J. Am. Chem. Soc.* **2005**, *127*, 4992−4993.
(68) Bour, P.; Keiderling, T. A. *J. Phys. Chem. B* **2005**, *109*, 5348−5357.
(69) Kim, J.; Huang, R.; Kubelka, J.; Bour, P.; Keiderling, T. A. *J. Phys. Chem. B* **2006**, *110*, 23590−23602.
(70) Ragothama, S. R.; Awasthi, S. K.; Balaram, P. *J. Chem. Soc., Perkin Trans.* **1998**, *2*, 137−143.
(71) Zhao, C.; Polavarapu, P. L.; Das, C.; Balaram, P. *J. Am. Chem. Soc.* **2000**, *122*, 8228−8231.

resulting in a tight left-handed turn that matches the preferred right-hand twist of the antiparallel strands.[72] However, this is not an optimal choice for isotopic substitution studies since the Xxx-Pro amide linkage has an amide I′ band at ~1611 cm^{-1} that spectrally overlaps the expected position of the $^{13}C{=}O$ peak of interest.[34] In this study, we substituted an Aib residue (aminobutyric acid or *R,R*-dimethyl glycine) into the Gellman sequence (Scheme 1) to initiate turn formation and stabilize hairpin formation[73] which results in spectral properties suitable for isotopic study.

Scheme 1. Design Structure of Gellman A Peptide Showing Numbering of Individual Residues in Sequence and $^{13}C{=}O$-Labeling Patterns (colored rectangles)

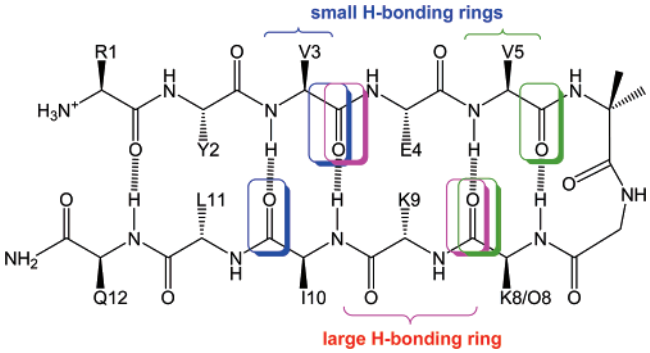

Density functional theory (DFT) calculations of model peptides have long been used to simulate IR and other peptide vibrational spectra.[50,68,72,74−81] The use of full optimization of the structure while constraining the (ϕ,ψ) angles to yield a specific model conformation has been successful in elucidating spectral characteristics of higher-frequency, amide-centered modes. Transfer of DFT calculated vibrational parameters allows calculations of the vibrational spectra for very large peptides, provided that they have regular repeating geometries.[77,82] In particular, the vibrational coupling (frequency splitting) of specifically labeled $^{13}C{=}O$'s for both α-helical and β-sheet peptides can be accurately predicted by DFT-based calculations,[37,50,58,68,74,75] which is useful for interpreting the isotopically labeled amide I′ spectral patterns in regular structures, but even more important for using the spectra of isotopically labeled peptides to elucidate their local structural changes. Lower-level semiempirical quantum chemistry calculations[32,81,83] have been also used to predict the vibrational couplings. For β-hairpin peptides realistic spectral simulations are complicated by the fact that the structures are not regular, since the antiparallel strands contain residues with very different (ϕ,ψ) angles due to both a turn between them and frayed termini. Additionally the β-strands are highly twisted.

DFT calculations based on a regular model geometry do not include the structural variation possible in a dynamically fluctuating hairpin. To overcome this limitation and better simulate the real molecule, we carried out DFT calculations on selected structures derived from long-time (~100 ns) molecular dynamics (MD) trajectories as well as from the NMR structure of the peptide.[69] Additionally we have used such trajectories to provide ensembles of structures for which we carried out classical (transition dipole) calculations of cross-strand coupling of labeled positions.[69] In this work, we will compare the experimental spectra to interpretations derived from these different theoretical simulations. A preliminary report on the spectra of some of these labeled molecules has appeared.[67]

Table 1. Model Peptide Sequences

Notation	Sequence [a]
U	RYVEVBGOKILQ-NH_2 [b]
V3	RY<u>V</u>EVBGKKILQ-NH_2
V5	RYVE<u>V</u>BGKKILQ-NH_2
I10	RYVEVBGKK<u>I</u>LQ-NH_2
V3K8	RY<u>V</u>EVBG<u>K</u>KILQ-NH_2
V3I10	RY<u>V</u>EVBGOK<u>I</u>LQ-NH_2
V5K8	RYVE<u>V</u>BG<u>K</u>KILQ-NH_2

[a] Underlined amino acid is $^{13}C{=}O$ labeled (Scheme 1). [b] B = Aib (aminoisobutyric acid or α,α-dimethylglycine), O = Orn (ornithine)

Materials and Methods

Peptide Synthesis and Purification. All peptides studied were synthesized at Louisiana State University on a Pioneer Peptide Synthesizer using four equivalents of amino acid and activation with TBTU, HOBt (final concentration of 0.25 M), and diisopropylethylamine (DIEA) at a final concentration of 0.5 M. A stepwise coupling of each amino acid was obtained using the standard solid-phase Fmoc coupling chemistry. Aib was double coupled using PyAOP as the coupling agent and DIEA as the activator (4 equiv and 0.2 M final concentration of PyAOP and amino acid) at an elevated temperature of 50 °C due to the difficult coupling of the sterically hindered Aib.[84,85] Additionally, the residue on the N-terminal side of the Aib, Val5 in this case, was also double coupled with PyAOP at 50 °C as above, due to the difficulty in acylating the hindered Aib amino group.[84−86] Labeled peptides were synthesized by using Fmoc-protected, side-chain protected (as appropriate) 1-^{13}C-labeled Fmoc-blocked amino acids purchased from Cambridge Isotope Laboratories (CIL), Inc. Fmoc-1-^{13}C-Ile-OH was prepared as previously described in our initial report.[67] Once the sequence was complete, the peptide was removed from the solid-phase resin by using a cleavage cocktail (by dissolving in 88:5:5:2 TFA/phenol/water/TIPS for 2 h). Crude peptides were isolated by precipitation into 10 volumes of cold ether, purified by reverse phase HPLC (purity ≥95%) and characterized by MALDI-MS. For clarity, we use the notations in Table 1 to designate the various positions labeled in the peptides used in this study. Lys (K) was substituted for Orn (O) in the original Gellman sequence for labeling convenience and has no structural or spectral consequence due to the similarity of K and O.

ECD Sample Preparation and Spectral Parameters. For ECD experiments, peptide solutions of ~0.15 mg/mL (~0.1 mM) in 20 mM phosphate buffer (pH ≈ 7) were prepared. Far-UV CD spectra were

(72) Bour, P.; Keiderling, T. A. *J. Mol. Struct. (THEOCHEM)* **2004**, *675*, 95−105.
(73) Aravinda, S.; Shamala, N.; Rajkishore, R.; Gopi, H. N.; Balaram, P. *Angew. Chem.* **2002**, *114*, 4019−4021.
(74) Kubelka, J.; Huang, R.; Keiderling, T. A. *J. Phys. Chem. B* **2005**, *109*, 8231−8243.
(75) Kubelka, J.; Keiderling, T. A. *J. Am. Chem. Soc.* **2001**, *123*, 6142−6150.
(76) Kubelka, J.; Keiderling, T. A. *J. Am. Chem. Soc.* **2001**, *123*, 12048−12058.
(77) Kubelka, J.; Silva, R. A. G. D.; Bour, P.; Decatur, S. M.; Keiderling, T. A. In *Chirality: Physical Chemistry*. Hicks, J. M., Ed.; ACS Symposium Series 810; American Chemical Society: Washington DC, 2002; pp 50−64.
(78) Bour, P.; Keiderling, T. A. *J. Phys. Chem. B* **2005**, *109*, 232687−23697.
(79) Jalkanen, K. J.; Jurgensen, V. W.; Claussen, A.; Rahim, A.; Jensen, G. M.; Wade, R. C.; Nardi, F.; Jung, C.; Degtyarenko, I. M.; Nieminen, R. M.; Herrmann, F.; Knapp-Mohammady, M.; Niehaus, T. A.; Frimand, K.; Suhai, S. *Int. J. Quantum Chem.* **2006**, *106*, 1160−1198.
(80) Choi, J.-H.; Kim, J.-S.; Cho, M. *J. Chem. Phys.* **2005**, *122*, 174903−174911.
(81) Choi, J.-H.; Hahn, S.; Cho, M. *Int. J. Quantum Chem.* **2005**, *104*, 616−634.
(82) Bour, P.; Sopkova, J.; Bednarova, L.; Malon, P.; Keiderling, T. A. *J. Comput. Chem.* **1997**, *18*, 646−659.
(83) Hahn, S.; Ham, S.; Cho, M. *J. Phys. Chem. B* **2005**, *109*, 11789−11801.
(84) Fu, Y.; Etienne, M. A.; Hammer, R. P. *J. Org. Chem.* **2003**, *68*, 9854−9857.
(85) Fu, Y.; Hammer, R. P. *Org. Lett.* **2002**, *4*, 237−240.
(86) Martin, L.; Ivancich, A.; Vita, C.; Formaggio, F.; Toniolo, C. *J. Pept. Res.* **2001**, *58*, 424−432.

acquired between 185 and 250 nm at 50 nm/min, with 1-nm bandwidth and 2-s response time on a JASCO J-810 spectrometer using a 1-mm quartz cell (Starna, Inc). As a test for concentration effects, spectra were also run at 20, 5, and 1 mg/mL. Final spectra were recorded as an average of eight scans and baseline subtracted. Variable-temperature experiments were done by monitoring the temperature of the sample holder heated by flow from a water bath (Neslab RTE7DP) with a 1 °C/min ramp speed and a 5-min equilibration time under control of a JASCO program. A set of 19 spectra over the range of 5−95 °C (in steps of 5 °C) was obtained for sample and buffer under identical experimental conditions, and subtractions for baseline correction were performed afterward. No smoothing was performed on the spectra before analysis.

IR Sample Preparation and Spectral Parameters. Purified peptides were lyophilized against 0.1 M DCl/D_2O solution (both DCl and D_2O from Sigma), redissolved in D_2O, neutralized by adding small aliquots of NaOD solution, and lyophilized again. Peptide solutions for IR studies were prepared with a range of concentrations, ∼10−46 mg/mL (∼7−32 mM), by dissolving lyophilized peptides in 20 mM deuterated phosphate buffer (pH 7, ≈ uncorrected). These peptides are quite soluble under the above conditions, and the data presented were normally obtained at ∼23 mg/mL with a 100-μm path length. As a test for concentration effects, spectra were also run at 20, 5, and 1 mg/mL.

IR spectra were acquired on a DigiLab FTS-60A spectrometer. Peptide solutions were sealed in a homemade demountable CaF_2 window cell having either a 50- or 100-μm Teflon spacer. All spectra (sample and background) were collected at a resolution of 4 cm^{-1} with a zero-filling factor of 8. Temperature-variation experiments were conducted with a homemade cell holder controlled from 5 °C to 95 °C by flow from a bath (Neslab RTE 111). The experiments were realized by simultaneous execution of two independent programs (DigiLab Resolution Pro for spectral scan and NEScom for temperature ramp). The sample was heated at 1 °C/min and equilibrated for 11 min, and then a 16-minute data collect (940 scans co-added) was accumulated before the next temperature step.

IR Spectral Simulations. A model β-hairpin peptide structure was derived from structural parameters for two strands of the β-sheet domain in the structure of intestinal fatty acid binding protein (PDB code: 1IFC) as has been described separately.[76,87] An NMR-based structure of the **U** peptide studied here[88] was also used to create another model for comparison calculations. The methods used to fragment the structure into smaller turn and strand components, to carry out DFT calculations of the spectral property tensors (force fields, and atomic polar tensors), and to transfer these onto the full hairpin structure have been previously described in detail.[34,69,82] DFT calculations of the force field and atomic polar tensors were done at the BPW91/6-31G** level for just the peptide framework (i.e., all Ala, no solvent) using the Gaussian 03 package. This level of computation has well-known limitations, but we have shown it gives qualitatively useful analysis of the amide IR spectra.[69,74,78] IR spectral patterns were simulated by assigning to each computed transition a band shape having a width of 10 cm^{-1} (fwhm) to best match the experimental resolution.

MD Simulations. Molecular Dynamics (MD) calculations were carried out in explicit water at temperatures ranging from 280 to 500 K. At each temperature several trajectories were simulated up to 100 ns. The simulation box used contains about 1500 SPC water molecules and the peptide of interest, which was modeled with OPLS-AA. An NVT ensemble was used by employing a Berendsen thermostat with a 0.1 ps coupling time. Simulations were performed using Gromacs 3.0 and 3.3.[89] The long-range interactions were implemented either with a simple 1.0 nm cutoff or with 1.0 nm cut offs and Particle Mesh Ewald (PME). The initial configuration was a folded model structure derived from an NMR-determined structure,[88] and the MD trajectories sampled several unfolding and refolding events, particularly at high temperatures. Conformations obtained from these trajectories provided alternative structural models for the spectral calculations.[69] For comparison with low-temperature experimental data, the conformational fluctuations were analyzed specifically for the parts of the trajectories where the peptide maintains an overall folded nature.

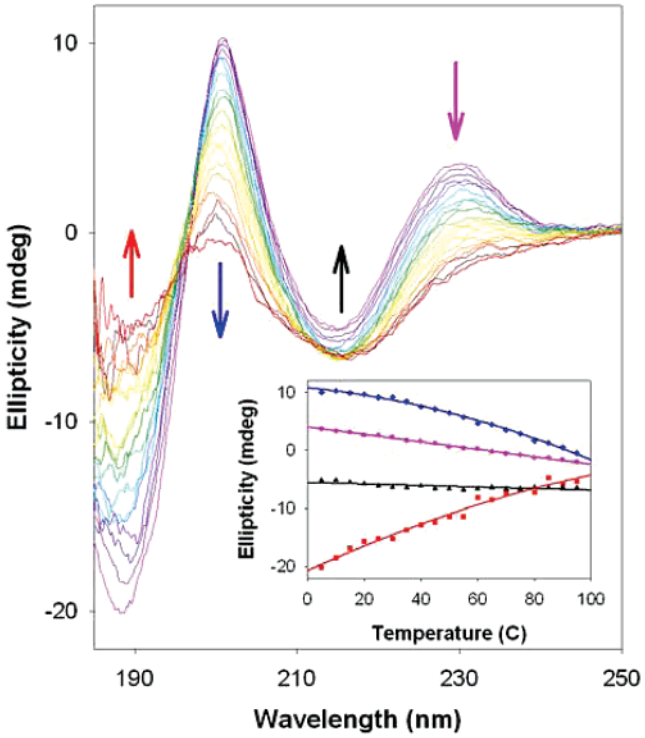

Figure 1. Temperature-dependent ECD spectra of the unlabeled peptide (**U**) measured from 5 to 95 °C. Peptide concentration is ∼0.15 mg/mL in 20 mM phosphate buffer. The path length of the cell is 1 mm. Arrows indicate direction of ellipticity changes with increasing temperature, which is color coded from violet (cold) to red (hot). (Inset) Ellipticity changes at various peak positions (color correlated to the arrows, 188 nm - red, 201 nm - blue, 215 nm - black, and 230 nm - pink) for the unlabeled peptide (**U**) shown with increasing temperature. Solid lines are the best fit for the data.

Results

ECD Thermal Unfolding. ECD spectra of all peptides were measured in 20 mM phosphate buffer (pH ≈ 7) to verify that they all adopted a β-hairpin conformation. All the peptides studied (the unlabeled and the labeled peptide variants) show identical band shapes, which are characteristic of β-sheet spectra (with a negative trough at ∼215 nm and a positive peak at ∼201 nm), but the positive peak is reduced in intensity due to overlap with a negative peak at ∼188 nm, echoing some features found in turns[90] (Figure 1). These shapes are independent of concentration up to 20 mg/mL, indicating freedom from aggregation effects. The aromatic residue (Tyr) in the peptide sequence gives rise to a weaker positive feature at 230 nm. Since isotopic substitution should have no effect on the ECD spectra, the identical nature of these spectra indicates all the peptides have the same fold. Added TFE did not further stabilize the β-hairpin conformation, but rather induced the peptide to form a partial

(87) Kubelka, J. Ph.D. Thesis. University of Illinois at Chicago, Chicago, 2002.
(88) Masterson, L. R.; Etienne, M. A.; Porcelli, F.; Barany, G.; Hammer, R. P.; Veglia, G. *Biopolymers* **2007**, *88*, 746−753.
(89) Lindahl, E.; Hess, B.; Spoel, D. v. d. *J. Mol. Model.* **2001**, *7*, 306−317.
(90) Rose, G. D.; Gierasch, L. M.; Smith, J. A. *Adv. Protein Chem.* **1985**, *37*, 1−109.

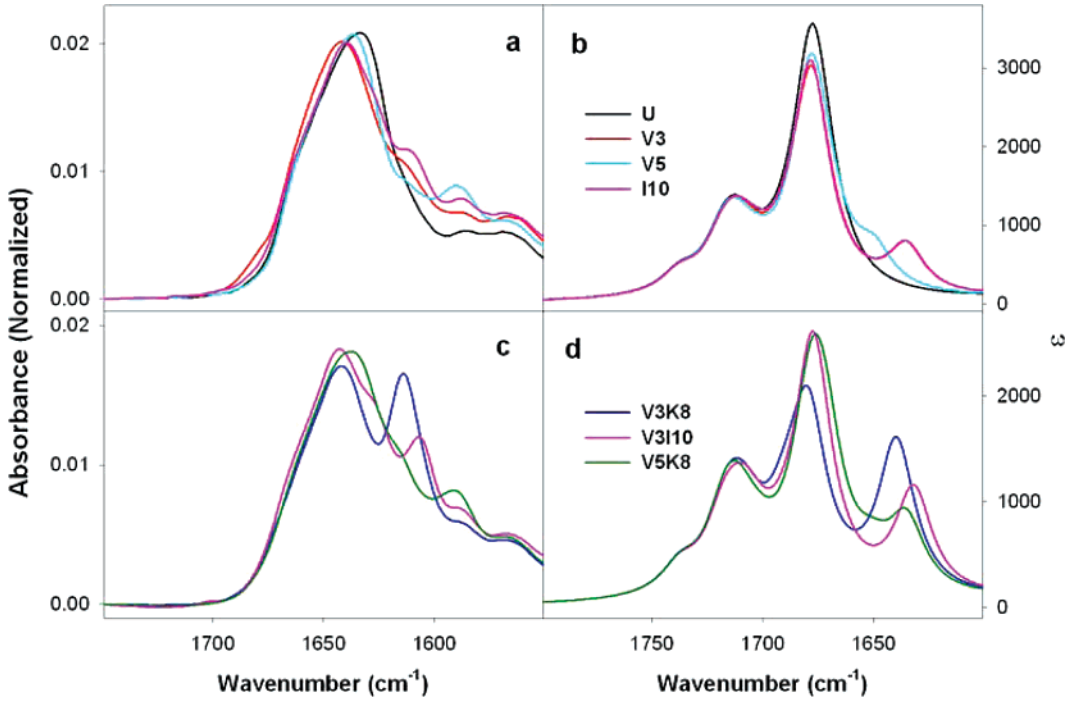

Figure 2. Experimental IR spectra of (a) the unlabeled and single-labeled hairpin peptides and (c) the double-labeled peptides. The experimental spectra were normalized to have a peak area of 1 between 1720 and 1550 cm^{-1}. The original spectra of all peptides were measured at ~23 mg/mL in 20 mM deuterated phosphate buffer in a 100 μm path length cell. Simulated IR spectra of Ac-A_{12}-$NHCH_3$ by transfer from shorter fragments are in (b) for the unlabeled peptide compared with single-labeled peptides **A3**, **A5**, and **A10** and (d) for the double-labeled peptides **A3A8**, **A3A10**, and **A5A8**.

α-helical-like conformation with a double minimum at 222 and 208 nm and a more intense positive peak at 193 nm (data not shown). This change is probably aided by the high helical propensity of Aib.[91]

The thermal stability of the secondary structure of the hairpin peptide in phosphate buffer was monitored by variable-temperature ECD (Figure 1). The overall band shape is preserved from 5 to 95 °C, but the characteristic peak intensities (for the features at 188, 201, and 230 nm) are much lower at high temperature, although there is little change in intensity for the negative band (β-structure) at ~215 nm. These results are very similar to the previously reported ECD for the closely related Gellman-designed 12mer β-hairpin peptide, ^{D}PG12 (RYVEV^{D}PGKKILQ).[33−35] The main positive peak shifts from 201 to 199 nm with increasing temperature and does not show a clear isodichroic point, which suggests an increasing contribution from residues in a disordered conformation. The broad thermal transition, as monitored by temperature-induced ellipticity changes at various wavelengths (Figure 1, inset), shows little curvature and suggests that the peptide does not undergo a simple two-state unfolding process. The high-temperature band shape indicates that the peptide retains some residual secondary structure in solution even at 95 °C.

Experimental and Simulated IR Spectra. Experimentally, the unlabeled β-hairpin gives rise to a broadened amide I′ IR band (D_2O solution) whose maximum is ~1633 cm^{-1} at 5 °C, which is consistent with formation of a partial antiparallel β-sheetlike cross-strand interaction (Figure 2a, black line). The shoulder peaks below 1600 cm^{-1} are contributions from the side-chain-originating absorption bands of arginine (~1585 cm^{-1}) and glutamic acid (~1568 cm^{-1}) at neutral pH.[56,92,93] On heating up to ~95 °C, the amide I′ band shifted to 1643 cm^{-1}, consistent with unfolding of the hairpin, and the two Arg side-chain absorption bands converge to a broad band at high temperature. Another Arg side-chain band appears at ~1608 cm^{-1} at high temperature.[56,93]

To expose the local unfolding process at specific sites, amide $^{13}C{=}O$ isotopic variants were prepared with single labels on **V3**, **V5**, and **I10** and double labels on **V3K8**, **V3I10**, and **V5K8**. However, before developing a model for the effect of conformational changes on the ^{13}C-labeled group vibrations, it is necessary to first understand the origins of the isotopic vibrational frequency shifts. The single labels provide data for identifying the local, position-determined frequency (diagonal force-field terms), and the double labels add the effects of the cross−strand vibrational coupling (off-diagonal terms) to them. The single-labeled **V3** and **V5** hairpins give rise to $^{13}C{=}O$ sidebands at ~1613 cm^{-1} (which for **V5** is weak, but obvious with deconvolution), and **I10** shows a sideband at ~1610 cm^{-1} (Figure 2a), or ~20−23 cm^{-1} below the maximum of the unlabeled hairpin. Additionally the main $^{12}C{=}O$ band shifts higher in frequency, increasing the $^{12}C{-}^{13}C$ gap, in a manner dependent on the substitution position.

The double-labeled variants have quite different $^{13}C{=}O$ patterns (Figure 2c). **V3I10** (whose labeled $^{13}C{=}O$ groups form a small, 10-member H-bonded ring) has a moderate intensity peak at 1607 cm^{-1}, while **V3K8** ($^{13}C{=}O$'s form a big, 14-member H-bonded ring) has a strong $^{13}C{=}O$ peak at 1614 cm^{-1}, or 7 cm^{-1} to higher frequency and more intense than

(91) Toniolo, C.; Crisma, M.; Formaggio, M.; Peggion, C. *Biopolymers* **2001**, *60*, 396−419.

(92) Barth, A. *Prog. Biophys. Mol. Biol.* **2000**, *74*, 141−173.
(93) Graff, D. K.; Pastrana-Rios, B.; Venyaminov, S. Y.; Prendergast, F. G. *J. Am. Chem. Soc.* **1997**, *119*, 11282−11294.

Table 2. Comparison of Experiment and Simulations for Labeled β-Hairpin Peptides

	experimental spectral peak[a]			simulated spectral peak[a]			computed normal modes[b]	
notation	^{12}C	^{13}C	difference	^{12}C	^{13}C	difference	^{13}C[d]	splitting
U	1633	N/A	N/A	1678	N/A	N/A	N/A	N/A
V3	1642	1613	29	1678	1636	42	1635	N/A
V5	1637	1614	23	1678	1650	28	1650	N/A
I10	1640	1610	30	1679	1636	43	1637	N/A
V3K8	1642	1614	28	1684	1641	43	1632 (w) 1640 (s)	+8
V3I10	1643	(1627[c]) 1607	16 36	1680	1633	47	1632 (s) 1640 (w)	−8
V5K8	1638	1616	22	1676	1636	40	1635 (m) 1651 (m)	−16

[a] Frequencies (in cm^{-1}) are determined from the original spectra as apparent maxima. No resolution enhancement used. [b] Frequency of individual component modes (in cm^{-1}). [c] This frequency corresponds to the shoulder peak. [d] Intensity of the normal modes (in parentheses): s - strong, m - medium, w - weak.

V3I10. These ^{13}C═O sideband results reflect predictions of our theoretical model (see below). The **V3I10** also has a weak shoulder at ∼1627 cm^{-1}, which could arise from the isotope-substituted positions disrupting ^{12}C═O coupling in the strands, as would explain the weaker, but similar shoulder in **I10**. For **V5K8**, the ^{13}C peak is only evident as a weak shoulder at ∼1616 cm^{-1}. These results are summarized in Table 2.

To better understand the role of isotopic labels on the IR spectra of the hairpin peptides, we have simulated IR spectra of a model β-hairpin initially using an idealized structure derived from a protein β-sheet segment (pdb 1IFC)[76] and compared them to our experimental IR spectra of the above peptides. In Figure 2b, the simulated amide I IR spectrum of the unlabeled peptide shows an intensity pattern typical of a sheet conformation, having an intense peak at low frequency (computed at ∼1678 cm^{-1}) and a weaker peak at high frequency (∼1737 cm^{-1}). The moderate band (1713 cm^{-1}) between these extremes corresponds to the non-H-bonded amide groups directed away from the other strand (out at the vacuum in this model). Our simulated spectra are not corrected for solvent (since they are derived from vacuum calculations on ideal hairpin segments, with Ala-based sequences) or for the expected errors for normal modes calculated with a DFT FF; thus, the computed amide I′ values are ∼45 cm^{-1} higher than the experimental ^{12}C═O maxima. Due to these solvation effects, in order to compare experimental and simulated ^{13}C═O effects, it is best to look at frequency differences which are compiled in Table 2 for the ^{13}C═O−^{12}C═O shift and for the ^{13}C═O coupling patterns for double-labeled species.

The ^{12}C═O experimental values do correspond to the expected lower-frequency component of a twisted β-sheet conformation.[72,75] The amide I′ frequency of a twisted pair of strands would be higher than for an extended, multistranded β-sheet with maximal coupling between strands.[75] For this reason the 1633 cm^{-1} amide I′ maximum of the unlabeled hairpin is higher than the amide I′ maximum observed at ∼1610 cm^{-1} in, for example, poly-Lys β-sheets.[94] The experimental IR spectrum of the unlabeled peptide (Figure 2a) is broader than the simulated ^{12}C amide I′ band but actually has less apparent dispersion, implying less exciton coupling due to nonuniformity of the β-strands. The broadness of the experimental ^{12}C═O band is presumably attributable to dynamic fluctuations between multiple conformations of the short, twisted β-strands arising from disorder at the frayed ends and to the strain and distortion involved in the turn.

When singly substituted with ^{13}C in the strands, the hairpin exhibits an additional peak (due to the isotopic effect) that is computed at ∼40 cm^{-1} lower-frequency than the main ^{12}C amide I band for **V3** and **I10**. The peptide **V5** has a single label next to the turn and is computed to have a 14 cm^{-1} higher ^{13}C frequency than do **V3** or **I10**, due to its poorly formed cross-strand H-bond. This is of course specific to the model structure chosen, and probably cannot be generalized. The diagonal FF can obviously vary significantly with position in the hairpin, which probably relates to local distortion in the model.

The spectra of the ^{13}C disubstituted peptides were also computed (Figure 2d). Although there are two components (normal modes) associated with the isotopic labeled carbonyls, only one ^{13}C peak is apparent in the computed spectra because of the relatively large difference in intensity for the two labeled components as computed with our model. For the double-labeling pattern forming a large H-bond ring (14-atom) such as **V3K8**, which is in the middle of the hairpin, the higher-frequency component is more intense. By contrast, the labels forming a smaller ring (10-atom), such as **V3I10** (in the middle of the hairpin) and **V5K8** (near the turn), have the lower component predicted to be more intense. The simulated ^{13}C═O peak positions of **V3K8** and **V3I10** result in an 8 cm^{-1} difference in the ^{13}C absorbance maxima of these two peptides due to their having opposite components of the pair being most intense in the IR. These results for the ^{13}C═O modes are also summarized in Table 2. In our idealized simulation, the **V5K8** ^{13}C peak is not the same as that for **V3I10**, suggesting its ^{13}C═O coupling is somewhat different than in **V3I10**. This again, as noted for the **V5** case, could be the result of local distortion of the structure near the turn. The computed ^{12}C peak frequencies for these labeled peptides do not vary much (except for **V3K8**) due to the introduction of labels, but the ^{12}C═O IR intensities decrease in proportion to the increase in the number of ^{13}C═O groups.

In Table 2, we have summarized the observed and predicted ^{12}C and ^{13}C peak frequencies and their differences along with computed normal-mode frequencies of the ^{13}C labels. Due to the absolute frequencies obtained for amide I′ modes with vacuum simulations being significantly higher than experimental values, difference frequencies offer the best basis of comparison. Single-labeled peptides **V3** and **I10** have a larger experimental ^{12}C−^{13}C frequency difference than **V5** (Table 2, column 4), but this is due to the **V5** ^{12}C═O frequency being lower, which probably reflects less disruption of the β-strand exciton coupling since the **V5** label is close to the turn. In the same sense, the double-labeled peptide **V3I10** has the largest isotope shift (if only considering the low-frequency ^{13}C peak), followed by **V3K8** and finally **V5K8**. Simulated spectra (Table 2, column 7) show the same trends but not for the same reasons. The single-labeled **V5** peptide again has the smallest difference frequency. In this case, the reduction is due to the ^{13}C═O mode being very high compared to the others. Most likely this unique ^{13}C═O mode results from a difference in the **V5** diagonal FF contribution, possibly due to its location next to the turn. The variations in the experimental ^{12}C═O mode frequencies may

(94) Yasui, S. C.; Keiderling, T. A. *J. Am. Chem. Soc.* **1986**, *108*, 5576−5581.

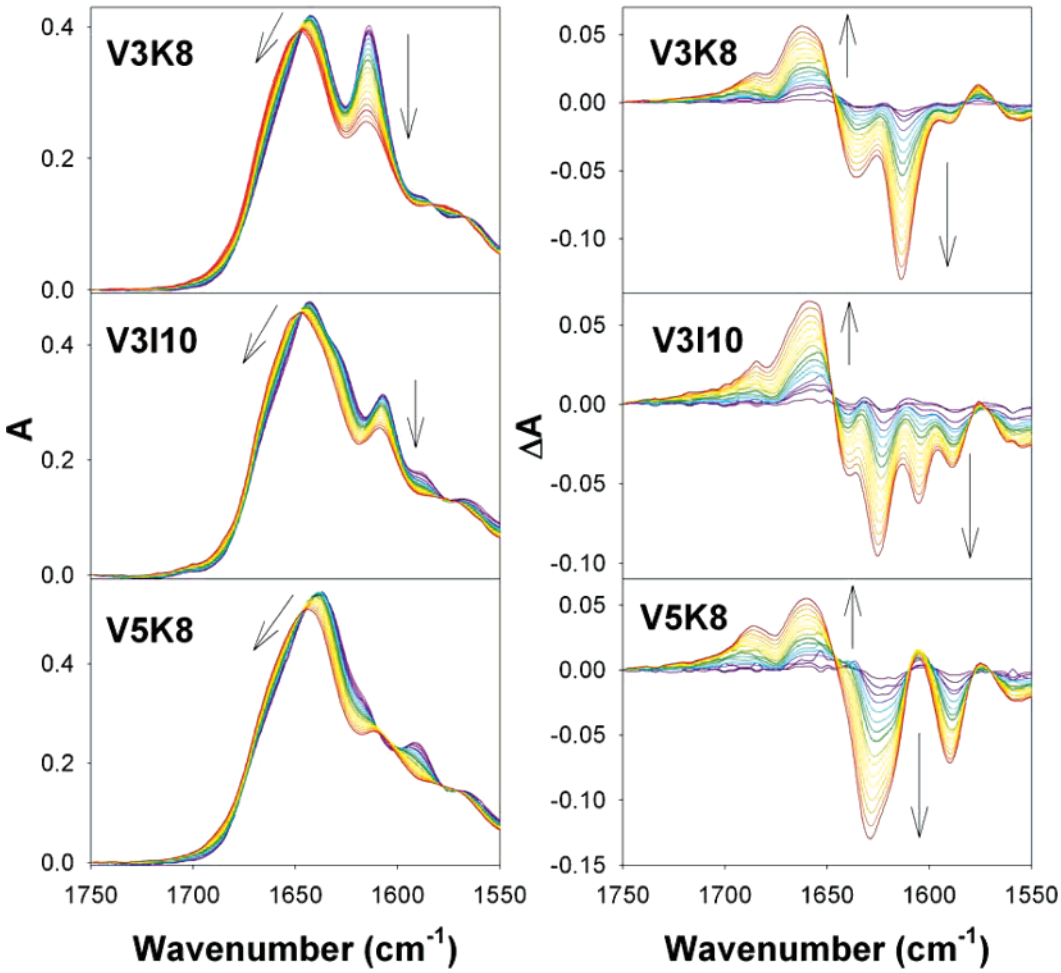

Figure 3. Original temperature-dependent IR spectra (left panels) and difference spectra (right panels) for double-labeled peptides **V3K8**, **V3I10**, and **V5K8**. All peptide concentrations were ~23 mg/mL in 20 mM deuterated phosphate buffer measured in a 100-μm path length cell. The difference spectra were taken by subtracting the spectrum at 5 °C from each spectrum at higher temperatures. In all panels the spectra are color coded for temperature, from blue at the cold (5 °C) extreme to red at the hot (95 °C) end, as suggested by the arrows.

reflect disruption of exciton coupling in the hairpin β-strands, which would lead to lower-frequency amide I′ maxima in longer β-strands. The comparisons made in this paper are for predicted and observed bandshapes, which are the basis of comparison of theory and experiment. Specific normal modes are not resolvable, particularly since the ^{12}C modes are all overlapped, so their individual characteristics cannot be derived from experiment. However, properties of selected decoupled modes can be inferred from the ^{13}C results. More details of the computed mode structure are available in the Supporting Information (Figures S1, S2).

The observed ^{12}C−^{13}C separations for the different label patterns are qualitatively reflected in our model calculations, but the details for specific modes under various labeling schemes are not as well predicted. This may be a result of our use of an idealized model. To address this, we have done DFT calculations on structures derived from MD simulations and from NMR experiments and have compared the predicted spectra based on those structures with our ideal hairpin structure simulation as previously reported (see Figure S1 in the Supporting Information).[69] Although the detailed mode distributions and magnitudes obtained for simulations with these alternate structures are not the same as for the ideal ones above, all models have a qualitative consistency in terms of predicted mode distribution, resulting in a ^{12}C amide I′ maximum in the lower frequency part of the band and an asymmetric shape. The key difference is that the ideal structure (as simulated in Figure 2) has its most intense mode (by a factor of 5) as one of the low-frequency components of the exciton band, whereas the more distorted structures result in a distribution of dipole strengths over the exciton components that gradually fall in intensity from low to high frequency (see Figure S1 in Supporting Information). This more distributed intensity pattern leads to a broadened amide I′ absorption pattern in better agreement with experiment than seen in Figure 2 for the idealized hairpin for the ^{12}C═O band. As for the isotope-labeled modes, all models have the same splitting for **V3K8** (big ring) and **V3I10** (small ring) but vary substantially in predicted coupling constant magnitude and yield less consistent results for **V5K8** (small ring), whose ^{13}C═O modes are dependent on the local conformation of the turn in each structure (Figure S2, in Supporting Information).

Thermal Unfolding by IR. To study the relationship of vibrational coupling and temperature-induced conformational change, the temperature-dependent FTIR were measured for all the peptides, and the amide I results for the double-labeled hairpin peptides are shown graphically in Figure 3 as original (left panels) and difference spectra (T − 5 °C) (right panels). The thermal unfolding process is quite reversible (data not

shown, for single-labeled hairpins see Figure S3 in Supporting Information). The main features of these spectra are (1) the frequency shift and small intensity loss of the main ^{12}C amide I′ peak and (2) the significant intensity change of the ^{13}C peak. While the low-temperature spectra varied sharply, depending on label positions as described above, at high temperature the amide IR of **V3K8**, **V3I10**, and **V5K8** are quite similar to each other. As temperature increases, the peptide unfolds from a more compact structure (β-hairpin) toward a less ordered structure (partial random coil), as evidenced by the upward frequency shift of the main ^{12}C amide I′ peak for all peptides (Figure 3, left panels). In the difference spectra this frequency shift appears as a decrease of the intensity at ~1630 cm^{-1} (negative difference) and an increase at ~1660 cm^{-1} (positive difference) (Figure 3, right panels), and the apparent band components have increased separation.

While the main ^{12}C amide I′ peak has similar behavior for all the labeled peptides, the ^{13}C═O band has a more variable thermal behavior. Of the three double-labeled peptides, **V3K8** has a single ^{13}C peak whose intensity change with temperature dominates the difference spectrum. **V3I10** has two new features arising from the ^{13}C labeling, one resolved, 1607 cm^{-1}, and the other a shoulder, ~1627 cm^{-1}. While the lower one is certainly a ^{13}C═O band, the higher one may be mostly ^{12}C═O in origin, reflecting the disruption of the exciton band by the ^{13}C label. This is supported by the similar, though weaker, pattern seen in the **I10** spectrum. Despite the presumably different mixing with the ^{12}C modes, these bands have similar T_m values. For **V5K8**, the ^{13}C features are overlapped in the difference spectra but are more evident in the normal spectra. A new peak at ~1608 cm^{-1}, also evident in **U** and **K5**, assignable to an Arg side-chain mode becomes resolved in going from low to high temperature.[56,93]

The amide I′ peak frequencies of the labeled peptides for the lowest experimental temperatures (T = 5 °C) fall into two groups (as shown in Figure 4, left axis). For **V5** and **V5K8**, the ^{12}C═O frequency is only ~3−4 cm^{-1} higher than for the unlabeled peptide (**U**), while for **V3**, **V3K8**, and **V3I10**, the ^{12}C peak is about ~8−9 cm^{-1} above **U**. The ^{12}C═O peak for **I10** lies somewhat between the groups. These differences show the effect of ^{13}C═O substitution(s) on the exciton coupling of ^{12}C═O's. However, the temperature-dependence of the ^{12}C═O peak is consistent for all peptides, as seen from the overall parallel behavior of their frequency shifts (Figure 4), which suggests that the same process is operative. Since the amide I frequencies for all the peptides do not converge even at 90 °C, the peptide does not appear to have reached a high-temperature steady state (disordered or unfolded form). This agrees with the ECD thermal unfolding data (Figure 1) where the intensities of the various bands changed but the spectral shapes did not. The absence of an upper baseline for these curves may imply less cooperativity in thermal unfolding; however, their obvious curvature did make it possible to attempt a fit of the data with a two-state model as an idealized, limiting test (Figure 4).

From results of the fit, **V5K8** would have a higher T_m than **V3K8** and **V3I10** (Table 3). The ^{12}C spectra have different contributions from turn and strand residues, depending on the positions of the labeled residues. Thus, the **V5K8** ^{12}C result will have more strand contribution, and its higher T_m suggests that the turn has less stability than the β-strands of this peptide.

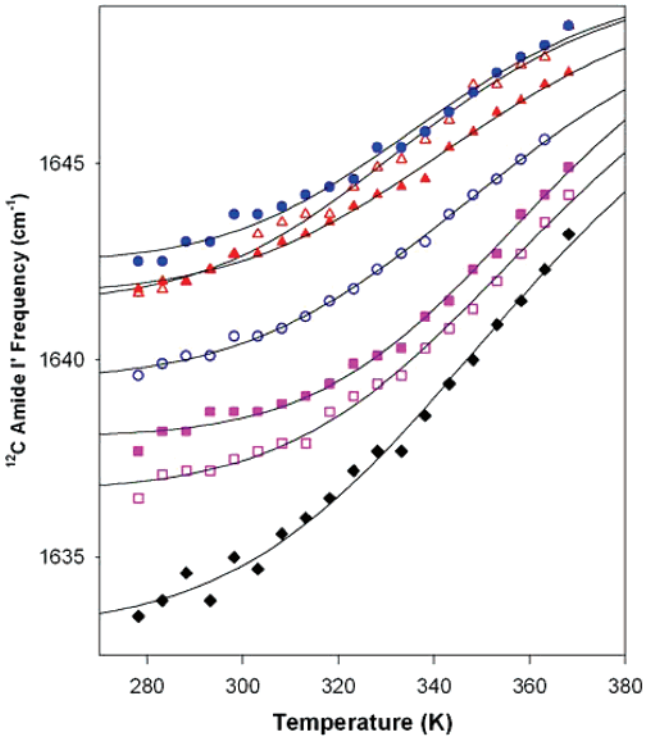

Figure 4. ^{12}C Amide I′ frequency shift with temperatures for **U** (black ◆), **V3** (red △), **V5** (pink □), **I10** (blue ○), **V3K8** (red ▲), **V3I10** (blue ●), and **V5K8** (pink ■). Solid lines are the best two-state fits for the data.

Table 3. Thermodynamic Parameters for Two-State Model Fit of Labeled Hairpin Unfolding

	monitored by amide I frequency shift		monitored by ^{12}C amide I intensity change		monitored by ^{13}C amide I intensity change	
	T_m (K)	ΔH (kJ/mol)	T_m (K)	ΔH (kJ/mol)	T_m (K)	ΔH (kJ/mol)
U	358 ± 16	8.3 ± 1.9	353 ± 5	13.3 ± 1.5	N/A	N/A
V3	337 ± 6	9.8 ± 2.0	352 ± 12	8.3 ± 1.5	335 ± 4	8.7 ± 1.1
V5	363 ± 13	9.6 ± 1.6	362 ± 6	12.6 ± 1.1	*a*	*a*
I10	354 ± 8	9.0 ± 1.1	361 ± 12	8.4 ± 1.2	331 ± 2	11.2 ± 1.1
V3K8	349 ± 8	9.3 ± 1.5	350 ± 6	12.7 ± 1.9	344 ± 3	7.6 ± 0.5
V3I10	340 ± 7	10.3 ± 2.2	347 ± 7	9.6 ± 1.4	343 ± 4	10.7 ± 1.1
V5K8	362 ± 11	11.0 ± 1.8	352 ± 5	18.1 ± 2.6	339 ± 11	4.1 ± 0.9

[a] Unrealistic fitting results were obtained.

By contrast, ^{13}C peak frequency shifts (data not shown) for **V3I10** and **V3K8** are of much less magnitude (~1 cm^{-1} shift) than for the main ^{12}C peak and do not yield a useful measure of the transition. **V5K8** is different; the frequency does shift, and the mode presumably changed character. The change has less contribution from cross-strand coupling due to the distortion of the H-bond next to the turn. However, their intensity changes are directly a consequence of the cross-strand coupling, which is lost on unfolding. Thus, we attempted to fit the apparent ^{13}C═O intensities as obtained from the original amide I IR data (e.g., Figure 3 and Figure S3 in Supporting Information). There was no advantage to use of the difference IR data for this analysis. The results are shown in Figure 5, and the analysis is summarized in Table 3.

Variations in ^{12}C peak and ^{13}C peak intensities (Figure 5) provide alternate probes of the thermal unfolding process, in which the **V3K8** and **V3I10** ^{13}C═O-labeled modes gain intensity by cross-strand coupling. Loss of intensity implies loss of order or increase in distance between residues on opposing strands.

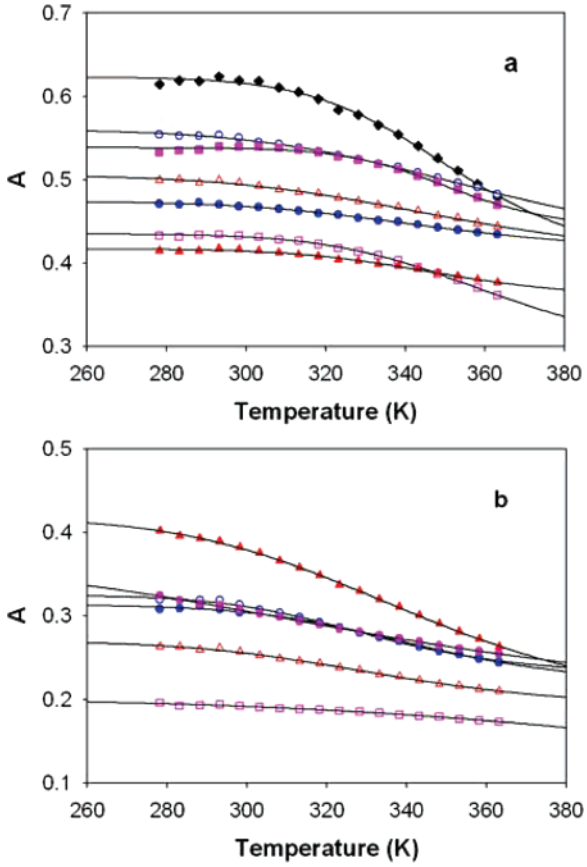

Figure 5. Two-state fit for (a) ^{12}C peak intensity change and (b) ^{13}C peak intensity change. Symbols are represented in the same way as in Figure 4. Solid lines are the best fit.

Although **V3K8** has the largest ^{13}C peak intensity change over this temperature range, the T_m values derived from analysis of the **V3K8** and **V3I10** $^{13}C{=}O$ intensity changes are very similar, and both are higher than the T_m from **V5K8**. Thus, the ^{13}C and ^{12}C results are consistent with the turn region having reduced stability, presumably due to distortion or strain in the hairpin, since **V5K8** is next to the turn.

Discussion

Aib-Gly Is a Stable Turn-Promoting Hairpin Formation. For this study Aib-Gly was substituted for ^{D}Pro-Gly in the original Gellman 12-residue β-hairpin peptide sequence[95,96] to avoid interference with the isotope-shifted IR band.[34] The IR spectra of the unlabeled peptide (**U**) confirm the ability of Aib-Gly to promote a turn, which then enables cross-strand H-bonding and leads to formation of a β-hairpin conformation as previously reported using X-ray crystallography,[73] and as now confirmed by NMR structural analysis.[88] The alignment of the hairpin strands is further confirmed by the $^{13}C{=}O$ labeling patterns and their close agreement with theory for **V3K8** and **V3I10**. However, even the low-temperature folded state has considerable distortion from regularity in the terminal residues and at the turn as demonstrated by our MD results for folded structures (see Figure S4 in Supporting Information) and by the lack of well-defined cross-strand coupling for **V5K8**.

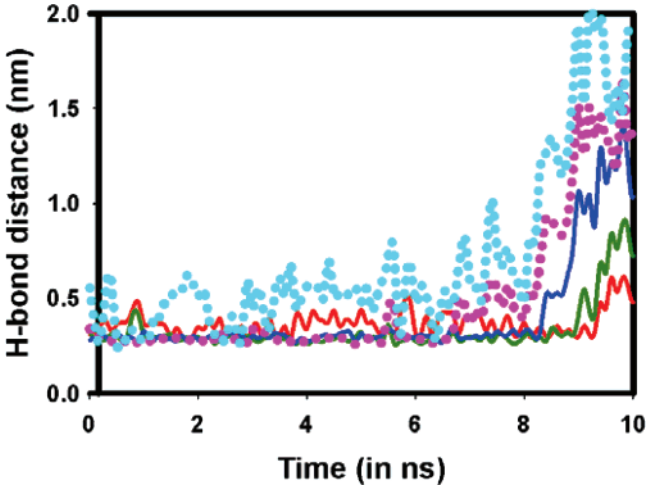

Figure 6. MD trajectory results showing H-bond distance fluctuation for a largely folded conformation at 300 K. Variations in the five H-bonds shown in Scheme 1 are indicated as: $V5^{C=O}{-}K8^{N-H}$ H-bond (red solid), $K8^{C=O}{-}V5^{N-H}$ H-bond (green solid), $V3^{C=O}{-}I10^{N-H}$ H-bond (blue solid), $I10^{C=O}{-}V3^{N-H}$ H-bond (pink dotted), and $R1^{C=O}{-}Q12^{N-H}$ H-bond (cyan dotted). The $R1^{C=O}{-}Q12^{N-H}$ H-bond fluctuation indicates the unfolding of the terminal residues, and the red line shows the $V5^{C=O}{-}K8^{N-H}$ H-bond next to the turn also fluctuates. Sequential opening of the H-bonds on unfolding is evident in this particular trajectory.

The stability of these Aib-Gly β-hairpins is comparable to that of peptide models based on the ^{D}Pro-Gly turn sequence.[34] Both hairpins have very broad unfolding transitions that remain incomplete at even 95 °C, confirming that some residual structure remains. Our simulations have shown these to occur in different sequential steps of which "unzipping" by sequentially losing H-bonds from the termini is one possibility (Figure 6).

Classical force field-based molecular dynamics (MD) simulations have been carried out by several labs to develop residue-level detailed understanding of β-hairpin formation.[16,18,19,29,97−103] The results varied, depending upon force fields, solvent model, simulation protocols, and the peptide system studied. However, the trajectories obtained and their analyses have increased our physical insights into β-hairpin structure in various compact states as well as the corresponding folding mechanisms. In addition, the MD simulations provide a basis for incorporating some effects of structural fluctuations[69] into quantum mechanical calculations of the vibrational spectra. Such combined approaches can provide more realistic simulations and therefore improve the interpretation of the experimental vibrational spectra. Our approach utilizes MD simulations, in particular, to sample local structural heterogeneity and conformational fluctuation but does not yet incorporate dynamics directly. The MD details have been reported with regard to spectral simulation[69] and will be communicated further regarding structural variation in separate publications (Kim and Keiderling, manuscript to be published).

Our MD simulations for this peptide show the turn region to remain somewhat compact (avoiding fully extended structures)

(95) Haque, T. S.; Gellman, S. H. *J. Am. Chem. Soc.* **1997**, *119*, 2303−2304.
(96) Syud, F. A.; Espinosa, J. F.; Gellman, S. H. *J. Am. Chem. Soc.* **1999**, *121*, 11577−11578.
(97) Bolhuis, P. G. *Proc. Natl. Acad. Sci. U.S.A.* **2003**, *100*, 12129−12134.
(98) Garcia, A. E.; Sanbonmatsu, K. Y. *Proteins* **2001**, *42*, 345−354.
(99) Klimov, D. K.; Thirumalai, D. *Proc. Natl. Acad. Sci. U.S.A.* **2000**, *97*, 2544−2549.
(100) Ma, B.; Nussinov, R. *Protein Sci.* **2003**, *12*, 1882−1893.
(101) Tsai, J.; Levitt, M. *Biophys. Chem.* **2002**, *101−102*, 187−201.
(102) Zhang, J.; Qin, M.; Wang, W. *Proteins* **2006**, *62*, 672−685.
(103) Zhou, R.; Berne, B. J. *Proc. Natl. Acad. Sci. U.S.A.* **2002**, *99*, 12777−12782.

although quite variable in detailed conformation even for highly folded structures. For short, lower-temperature trajectories (such as seen in Figure 6, and as expanded in S4, Supporting Information), the folded hairpin contains all the expected H-bonds. The terminal bond and the turn H-bond show much more fluctuation, as was noted above, until the hairpin unfolds.

By contrast, higher temperature trajectories lead to "fully unfolded" conformers which have no cross-strand H-bonds.[69] Such MD trajectories begun from an unfolded hairpin (for example Figure S5 in Supporting Information) occasionally show refolding to a partially formed structure with frayed termini and formation of a type I′ turn. However even when unfolded, as seen in the bottom of Figure S5 in Supporting Information, the ϕ,ψ angles of the Aib indicate that its conformation is mostly contained in this part of Ramachadran space ($\phi \approx 60°$, $\psi \approx 30°$) with little correlation to the overall folding as represented by the H-bond structure. Although the turn region is compact, considerable fluctuation remains which leads to multiple deformations of the $V5^{C=O}-K8^{N-H}$ H-bond since the geometries of these residues fluctuate widely.

Our simulations regularly show that the H-bond closest to the turn separates and the residues close to the turn to have a wider variance than those in the center of the antiparallel strands. This is best seen in the H-bond distance distribution plots which show the H-bond from $K8^{N-H}$ to $V5^{C=O}$ to have a broad distribution and peak at ~0.33 nm, while those in the center of the hairpin are narrow and peak at ~0.29 nm for $T = 300$ K (Figure S6 in Supporting Information).[69] The result of this fluctuation is a reduced average amide $^{13}C{=}O$ coupling for the labeled positions in **V5K8**. The trajectories we have simulated imply the central residues of the hairpin strand region have relatively high uniformity, in comparison to the fraying of the termini and twists and the fluctuations of the turn even at moderate temperatures. Consequently the **V3I10** and **V3K8** labeled peptides have strongly coupled $^{13}C{=}O$ groups resulting in well-defined and intense isotopic shifted bands.

Isotope Editing Probes Strength of Vibrational Couplings. From simulation results, different isotopic labeling patterns showed distinct spectral effects. In our model peptide, there are two kinds of double ^{13}C-labeling patterns: 14-member H-bond ring (big ring) and 10-member H-bond ring (small ring), as seen in Scheme 1. The labeling pattern resulting in a big ring gives a ^{13}C band with higher intensity and a higher frequency (less separation from the ^{12}C band, e.g., **V3K8**), while the alternate labeling pattern resulting in a small ring gives a ^{13}C band with much lower intensity at a lower frequency (more separation from $^{12}C{=}O$, e.g., **V3I10**). That ^{12}C modes mix at a low level with ^{13}C modes is suggested by the strong ^{13}C peak intensity seen for **V3K8**, since the relative peak height is much larger than the ^{13}C:^{12}C ratio (2:10) would suggest. By contrast, there appears to be much less ^{13}C:^{12}C mode mixing for **V3I10**, which may result from the intense component of the coupled isotope modes being separated more from the main $^{12}C{=}O$ peak.

In model β-sheet calculations,[68] the predicted coupling of $^{13}C{=}O$ for a large ring was less than for a small ring which is reasonable because the distance between the two ^{13}C-labeled carbonyls is normally less in the small ring. Transition dipole coupling (TDC) in particular, varies inversely with distance ($\sim R^{-3}$), thus making the small ring coupling stronger. Since our idealized β-hairpin model was based on a regular β-sheet structure (derived from PDB: 1IFC)[67] but incorporated a small shift of the strands relative to each other, the distance between the oxygen atoms of the two labeled carbonyls were about the same for the big and small rings, and the resultant splitting was almost the same as reported previously.[67] However, in both cases, and in fact for all antiparallel models, opposite sign patterns are obtained for the coupling of C═O pairs in small (+) and large (−) H-bonded rings, even if only TDC is used for the computational model.[68,69] For the structures derived from MD or NMR the frequency shift patterns are the same, but the predicted intensity of the two components of the $^{13}C{=}O$ band are more similar than in the ideal case, which has maximal intensity difference of in- and out-of-phase $^{13}C{=}O$ modes due to its local symmetry that derives from the two triamide-strand basis used to construct the idealized model and transfer the vibrational tensor parameters,[68,82] as opposed to the fragmentation method used for the NMR and MD structures.[69,78] We have shown separately that the distribution of coupling constants (from a TDC model) for an ensemble of compact partially folded states had distinctly different peak values and dispersions for the three double-labeled sequences.[68,69] These dynamically sensitive results again fit the differential spectra observed between **V3K8** (less ^{13}C shift, higher intensity) and **V3I10** (more ^{13}C shift, lower intensity) that we saw (Figure 2) for the idealized hairpins, which directly results from their having oppositely signed $^{13}C{=}O-{}^{13}C{=}O$ coupling. The phase difference seen in these two coupling patterns is critical, since it leads to the frequency difference observed in all models, which is confirmed by experiment. This characteristic isotopic shift additionally confirms the proper antiparallel alignment of the strands by use of IR data alone.

In experiments, we did see a strong ^{13}C peak in **V3K8** that is higher in frequency than for **V3I10**, but we saw more complex spectral features in the latter. The "extra" band in **V3I10** (at ~1627 cm^{-1}) probably arises from a breakdown of the $^{12}C{=}O$ exciton coupling by $^{13}C{=}O$ substitution in the middle of a strand (especially the I10 position). One might ascribe it to nondegenerate diagonal FF contributions due to the location of $^{13}C{=}O$ oscillators, since **I10** probably becomes involved with the frayed N- and C-termini (as suggested by MD simulation, which showed that the outer two H-bonds in this hairpin are not stable[69]).

Our simulation also predicted that the two ^{13}C-labeled carbonyls forming a small ring near the β-turn (**V5K8**) are nondegenerate because the two carbonyls are easily distorted away from an orientation resulting in a good coupling. Consequently, the frequencies computed for these two modes are essentially the same as those of the individual single carbonyls when labeled. The validity of this prediction was confirmed by the weak shoulder seen for the $^{13}C{=}O$ contribution in **V5K8**, which is much the same as for **V5**. By extension, the failure to see a clear coupled $^{13}C{=}O$ band in the **V5K8** labeled hairpin confirms distortion of the turn region.

The secondary effect of substituting ^{13}C isotopes on the $^{12}C{=}O$ peak frequency can also yield site-specific conformational information. We have done some calculations of spectral patterns expected for structures derived from MD trajectories that had either all five H-bonds formed or only two or three H-bonds formed in the hairpin structure. For single-labeled peptides, **V3** and **I10** are located in the midst of the remaining

extended β-strand region; however, **I10** is closer to the frayed termini (in the case of two or three remaining H-bonds in the hairpin), and thus **I10** should have less effect on the $^{12}C{=}O$ exciton coupling than **V3**. This suggests that **I10** would have an amide I′ frequency closer to that of the unlabeled peptide than would **V3** (much as seen experimentally, Table 2). Since **V5** is located near the turn, it would have much less impact on the interstrand coupling, and thus its $^{12}C{=}O$ should be even more like **U** (again as seen experimentally). Overall, the order of breaking $^{12}C{=}O$ exciton couplings due to single $^{13}C{=}O$ substitution is **V3** > **I10** > **V5**. Considering the double-label cases, we see a shift up in frequency for the apparent $^{12}C{=}O$ band that mimics experiment for the more fully folded of the MD structures modeled, but the differences in the patterns are small between various structures. Our experimental data suggest that the low-temperature vibrational coupling in our peptide is dependent on the unique strand geometry that represents an energy minimum which may be best reflected by a combination (ensemble) of variably distorted (partially unfolded) models (ideal β-hairpin and frayed β-hairpin).

Isotope-Editing Reveals Site-Specific Stability. Optical spectroscopy can normally only monitor global structural changes in proteins and peptides. With isotopic labeling, one could in principle differentiate local conformational change at a residue level (site specific), which could greatly improve the understanding of protein-folding mechanisms and local structure. Here we have used the labels to discriminate turn and strand stability, being "regiospecific" through cross-strand coupling rather than strictly site specific.

Generally, a frequency shift of the amide I′ IR is expected when proteins/peptides undergo a conformational change because different secondary structural components have characteristic amide I frequencies. The low-temperature unlabeled β-hairpin peptide ^{12}C amide I′ peak at $\sim$1633 cm^{-1} shifts gradually to $\sim$1643 cm^{-1} as temperature is increased, which indicates a more dominant disordered conformation. Some of this frequency shift must result from the change in solvation of various sites changing environments from the folded peptide, with cross-strand H-bonded residues, to the unfolded variant, with primarily solvent H-bonded residues. Solvent shifts of peptide IR frequencies have been well studied, and we have explicitly modeled spectral changes in sheet structures, showing that the exposed C═O groups on the edge will have the largest changes.[34,68,78] Those residues with H-bonds to other strands will have less spectral shift upon interacting with solvent molecules. The edge residues have variable access that is a function of sequence, and these all contribute to the ^{12}C band, resulting in its width and part of its frequency shift on unfolding that reflects more global (solvation, in this case) effects. However, in our models, the ^{13}C-labeled residues are all cross-strand H-bonded at low temperature and thus have much less solvent effect. Thus, they have the potential to provide local probes of structure with less global impact.

IR spectra show a difference in behavior for the $^{12}C{=}O$ frequency and $^{13}C{=}O$ intensity with temperature and thus can provide site-specific information about the effect of the unfolding on vibrational coupling. The main amide I frequency change with temperature for the labeled peptides is indicative of a temperature effect on the $^{12}C{=}O$ exciton coupling since this is directly affected by ^{13}C substitution. The $^{13}C{=}O$ interruption of the $^{12}C{=}O$ exciton is smaller when labeled at **V5K8**; thus, the $^{12}C{=}O$ band in that case samples more of the antiparallel strand and the T_m derived is higher than for **V3K8** and **V3I10** (Table 3). Thus, the $^{12}C{=}O$ thermal changes in the latter cases tend to reflect the contributions of the turn and terminal groups more than for the **V5K8** or for **U**, the unlabeled case. On the other hand, the $^{13}C{=}O$ peak intensity change reports on the temperature variation of coupling of the labeled positions, thus giving more direct site-specific stability information. The ^{13}C peak intensity change for **V3K8** with increased temperature demonstrates that the vibrational coupling is significantly affected. There is strong vibrational coupling between the two $^{13}C{=}O$ modes at low temperature (when the peptide is in a β-hairpin conformation), and this is lost as the distance of the two $^{13}C{=}O$ groups is increased and/or the orientation is randomized when the peptide unfolds.

On the contrary, if the vibrational coupling were weak, the effect of temperature would be much smaller. Since the peptide contains labels that act as dipolar oscillators in both folded and unfolded states, the relevant change that accompanies unfolding is loss of cross-strand coupling. This is what we see in Figure 3. **V3I10** has two labels at positions that could be influenced by fraying of the ends, and **V5K8** has two labels at positions close to the turn, whereas **V3K8** is labeled in the antiparallel strand. This results in differences between the low-temperature spectra, even for the small-ring labeling in **V5K8** and **V3I10**. As temperature increases, the peptide unfolds so that all positions become disordered, and there is little differentiation between labeling sites; each is locally disordered, and there is no significant cross-strand coupling. Thus, the final, high-temperature spectra of all these peptides are very similar both for the $^{13}C{=}O$ and $^{12}C{=}O$ peaks, demonstrating unfolding of the strands at high temperature. The $^{13}C{=}O$ intensity changes have roughly similar T_m for the three double-labeled hairpins which suggests that these local labels sense the antiparallel strands and, for this example, do not differentiate between one end or the other.

Conclusions

We have systematically studied a series of β-hairpin peptides with isotope-edited IR spectroscopy. The peptide with Aib-Gly in the sequence as a turn-initiating segment shows very stable β-hairpin conformation over a wide temperature range. Different isotopically labeled variants of the β-hairpin peptide show different patterns of vibrational coupling, which is affected by the geometry of the peptide. Thermal unfolding experiments reveal that the vibrational coupling is sensitive to temperature. ^{13}C substitutions also affect residual ^{12}C couplings as monitored through frequency shifts and intensity variations. These effects are correctly predicted by theoretical DFT-based simulations for an idealized β-hairpin. In particular, the sign variation of the vibrational coupling between the cross-strand amides in the small and large H-bonding rings produces significant frequency shifts of the ^{13}C-labeled bands which can be used to confirm the registration of the antiparallel strands in the hairpin.

Acknowledgment. This research was originally supported by a grant from the National Science Foundation (CHE03 16014 and CHE07 18543 to T.A.K.) and from the National Institutes

of Health (AG17983 to R.P.H.) and ACS PRF (42027-AC4 to R.P.H.). Parts of this study were developed while T.A.K. was a Fellow of the John Simon Guggenheim Foundation. We thank Catherine L. Thomas and Martha Juban in the LSU Protein Facility for expert technical assistance in peptide synthesis and purification and Ling Wu at UIC for help in confirming spectral data.

Supporting Information Available: Detailed results from MD simulations, QM spectral calulations, and temperature-dependent IR spectra for the unlabeled and single-labeled peptides. This material is available free of charge via the Internet at http://pubs.acs.org.

JA0736414